



A spatially dynamic network underlies the generation of inspiratory behaviors

Nathan A. Baertsch^{a,1}, Liza J. Severs^a, Tatiana M. Anderson^a, and Jan-Marino Ramirez^{a,b,c,1}

^aCenter for Integrative Brain Research, Seattle Children's Research Institute, Seattle, WA 98101; ^bDepartment of Neurological Surgery, University of Washington, Seattle, WA 98104; and ^cDepartment of Pediatrics, University of Washington, Seattle, WA 98195

Edited by Peter L. Strick, University of Pittsburgh, Pittsburgh, PA, and approved March 7, 2019 (received for review January 16, 2019)

The ability of neuronal networks to reconfigure is a key property underlying behavioral flexibility. Networks with recurrent topology are particularly prone to reconfiguration through changes in synaptic and intrinsic properties. Here, we explore spatial reconfiguration in the reticular networks of the medulla that generate breathing. Combined results from in vitro and in vivo approaches demonstrate that the network architecture underlying generation of the inspiratory phase of breathing is not static but can be spatially redistributed by shifts in the balance of excitatory and inhibitory network influences. These shifts in excitation/inhibition allow the size of the active network to expand and contract along a rostrocaudal medullary column during behavioral or metabolic challenges to breathing, such as changes in sensory feedback, sighing, and gasping. We postulate that the ability of this rhythm-generating network to spatially reconfigure contributes to the remarkable robustness and flexibility of breathing.

breathing | dynamic network | rhythm generation | pre-Bötzinger complex

From as early as the pioneering work of Ramón y Cajal, anatomical and electrophysiological investigations have sought to compartmentalize brain regions based on the properties of neurons contained within them (1). Testing functional hypotheses for a given brain region has been commonly achieved by implementing lesion and stimulation experiments to determine whether the region is necessary or sufficient for a given behavior (2–4). This approach has contributed greatly to our understanding of brain function, while supporting the general view that the brain is organized into discrete anatomical and functional modules that underlie distinct behaviors (5).

The introduction of modern genetic, imaging, and optogenetic tools has led to an exponential increase in our insights into the functional anatomy of defined neuronal regions in vertebrate (6–9) and invertebrate model systems (10–13). However, neuronal circuit functions are often dynamic, state dependent (14–20), multifunctional (21–24), and task dependent (25). Mechanisms of experience-dependent plasticity can shift the spatial distribution of a neuronal network over time (26), and the topology of active brain networks can also dynamically reconfigure on rapid timescales (27, 28). In particular, networks with recurrent connectivity, such as motor cortex, appear to reconfigure by regulating the balance of excitation and inhibition to control the spread of neuronal activity through the network (26, 29, 30). However, while many mammalian studies are consistent with network reconfiguration, it is often difficult to define these dynamic changes at the cellular level.

The neuronal network controlling breathing offers a unique opportunity to characterize neural network dynamics in great detail (31). A series of studies identified the pre-Bötzinger complex (preBötC), a small “core” (32, 33) or “kernel” (34) network, which is critical for generating inspiration. Acute silencing of the preBötC causes apnea (4, 33), and when isolated in a thin medullary slice from neonatal rodents, it continues to produce a rhythm (35). Rostral to the preBötC, inhibitory neurons active during expiration were identified in the so-called Bötzinger complex (BötC) (36), and caudal to the preBötC, a region referred to as the ventral respiratory group (VRG) was found to contain bulbospinal

inspiratory and expiratory neurons thought to primarily serve premotor functions (37). These observations led to the respiratory network being described in terms of a series of discrete, rostrocaudally oriented “compartments,” the BötC, preBötC, and VRG (38–41).

However, there are no easily defined anatomical borders within the medullary respiratory network or between the hypothesized compartments. A rich array of recurrent connections (42), in particular among excitatory neurons derived from Dbx1-expressing progenitors (referred heretofore as “Dbx1 neurons”), is considered a critical property of the preBötC that gives rise to the inspiratory rhythm (33, 43). However, Dbx1 neurons extend far beyond the preBötC along the rostrocaudal axis of the ventral respiratory column (VRC) (43–45). Moreover, neuron types and spiking patterns are not homogeneous within each VRC compartment. Inhibitory neurons active during expiration, thought to characterize the BötC, are also found within the preBötC (43, 46, 47). Conversely, neurons active during inspiration are prevalent within the BötC, but also extend rostrally (48, 49). This may explain why, in some cases, lesions of the preBötC have failed to eliminate all inspiratory behaviors (50–52). Thus, evidence suggests that neurons important for inspiratory rhythmogenesis may not be limited to a discrete preBötC kernel.

Using optogenetic and electrophysiological techniques, we investigate the generation of inspiration in the wider medullary network and test the hypothesis that the spatial extent of inspiratory activity generated by the preBötC can dynamically reconfigure. We find that inspiratory activity along a distributed column of excitatory neurons is regulated by inhibition and that this distribution expands rostrally from the preBötC during changes in sensory feedback or inspiratory behaviors such as sighs and gasps. We postulate that this

Significance

Breathing is a vital rhythmic behavior that originates from neural networks within the brainstem. It is hypothesized that the breathing rhythm is generated by spatially distinct networks localized to discrete kernels or compartments. Here, we provide evidence that the functional boundaries of these compartments expand and contract dynamically based on behavioral or physiological demands. The ability of these rhythmic networks to change in size may allow the breathing rhythm to be very reliable, yet flexible enough to accommodate the large repertoire of mammalian behaviors that must be integrated with breathing.

Author contributions: N.A.B. and J.-M.R. designed research; N.A.B., L.J.S., and T.M.A. performed research; N.A.B. analyzed data; and N.A.B. and J.-M.R. wrote the paper.

The authors declare no conflict of interest.

This article is a PNAS Direct Submission.

This open access article is distributed under [Creative Commons Attribution-NonCommercial-NoDerivatives License 4.0 \(CC BY-NC-ND\)](https://creativecommons.org/licenses/by-nc-nd/4.0/).

¹To whom correspondence may be addressed. Email: nathan.baertsch@seattlechildrens.org or jan.ramirez@seattlechildrens.org.

This article contains supporting information online at www.pnas.org/lookup/suppl/doi:10.1073/pnas.1900523116/-DCSupplemental.

Published online March 27, 2019.

dynamic network architecture allows the size of the active recurrent network to be adjusted on a cycle-to-cycle basis, endowing the breathing rhythm with remarkable robustness and flexibility during ever-changing behavioral, metabolic, and environmental demands.

Results

Characterization of Inspiratory Activity in a Horizontal Medullary Slice. To explore inspiratory activity in the wider medullary network, we developed a horizontal brainstem slice preparation that encompasses the entire rostrocaudal extent of the ventral medulla (2) (*SI Appendix, Fig. S1 A–D*). Landmarks used to locate the preBötC in vivo (43) are preserved on the ventral surface of horizontal slices and corresponded to a location ~1,800 μm caudal to the VII nerve (rostral edge of the slice) and ~950 μm lateral from the midline. Horizontal slices prepared from male and female transgenic mice expressing fluorescent protein in cholinergic neurons confirmed that this location correlated with the known position of the preBötC relative to other neuronal landmarks such as the nucleus ambiguus (NA), facial nucleus (VII), and post-inspiratory complex (PiCo) (*SI Appendix, Fig. S1E*). This region also contained Dbx1-derived neurons (*SI Appendix, Fig. S1F*) known to be necessary and sufficient for generation of the inspiratory rhythm. However, as previously suggested (44, 45), these neurons extended along a rostrocaudal column, far beyond the preBötC. To further localize the preBötC in the horizontal slice, inspiratory modulated extracellular spiking activity was systematically mapped (*SI Appendix, Fig. S1G*). Beginning at the anatomical coordinates corresponding the preBötC center, maximal integrated inspiratory activity was recorded in 100- μm steps across the surface of horizontal slices. Inspiratory population activity spanned $1,488 \pm 199 \mu\text{m}$ in the medulla and could be recorded up to $625 \pm 106 \mu\text{m}$ rostral of the preBötC center.

To determine how integration of the preBötC within the wider rostrocaudal medullary network influences rhythmogenesis, we compared preBötC inspiratory activity generated in horizontal slices with preBötC activity generated in conventional transverse brainstem slice preparations (32) (Fig. 1A and *SI Appendix, Fig. S1H*). On average, horizontal slices ($n = 40$) produced a slower inspiratory rhythm with longer duration bursts (inspiratory time), longer pauses between bursts (expiratory time), and a longer time to reach peak burst amplitude (time to peak) compared with transverse slices from neonatal mice of a similar age [postnatal day 7 (P7) to P10; $n = 41$] (Fig. 1B and *SI Appendix, Fig. S1I*). Although horizontal slices had a slightly more irregular period,

horizontal slices exhibited much less irregularity in burst amplitude and burst area than transverse slices (Fig. 1C and *SI Appendix, Fig. S1J*), suggesting that horizontal slices produce a relatively robust and more synchronized rhythm compared with slices that isolate the preBötC. Because stronger synchronization within the preBötC leads to longer refractory periods following inspiratory bursts (43, 53), we compared the refractory period in horizontal ($n = 5$) and transverse ($n = 4$) slice preparations (Fig. 1D and E). Using Dbx1^{CreERT2};Rosa26^{Chr2-EYFP} mice, preBötC Dbx1 neurons were optogenetically stimulated contralateral to the extracellular electrode at random time points during the inspiratory cycle. Shortly following spontaneous preBötC bursts, the probability of photoevoking a subsequent burst (200 ms, 470 nm, 0.5 mW/mm²) was low in both horizontal and transverse slice preparations, indicative of refractoriness (43, 54). The probability of evoking a burst increased with time but was more delayed in horizontal slices, with a >80% chance of evoking a burst at 1.25 and 2.75 s in transverse and horizontal slices, respectively. Together, these results suggest that, when integrated within the wider medullary network, the preBötC generates a more robust rhythm associated with increased refractoriness.

A Distributed Heterogeneous Inspiratory Network. Next, we used the horizontal slice preparation to characterize the cellular determinants of the inspiratory rhythm along its rostrocaudal axis. Respiratory modulated neurons were selected for intracellular recording using the blind patch technique. The electrophysiological activity of each neuron was characterized in relation to preBötC population bursts, the anatomical location of each neuron was mapped using patch pipettes containing a fluorescent marker, and each neuron was classified as excitatory or inhibitory based on optogenetic stimulations (*SI Appendix, Fig. S2 A and B*). Electrophysiological activity patterns of respiratory neurons recorded in the horizontal slice fell into three main groups: inspiratory, expiratory, and postinspiratory. Locations of inspiratory and expiratory neurons and example spike raster plots of respiratory neurons during 30 consecutive inspiratory bursts are shown in Fig. 2. Respiratory neurons along the horizontal slice were primarily inspiratory, that is, maximum firing rates occurred in phase with preBötC population activity (47 of 65 neurons). However, there was considerable heterogeneity among inspiratory neurons. In support of previous findings (43, 55), inspiratory neurons were almost evenly split between excitatory and inhibitory (22 of 47 were inhibitory). Interestingly, inhibitory inspiratory neurons generally exhibited a

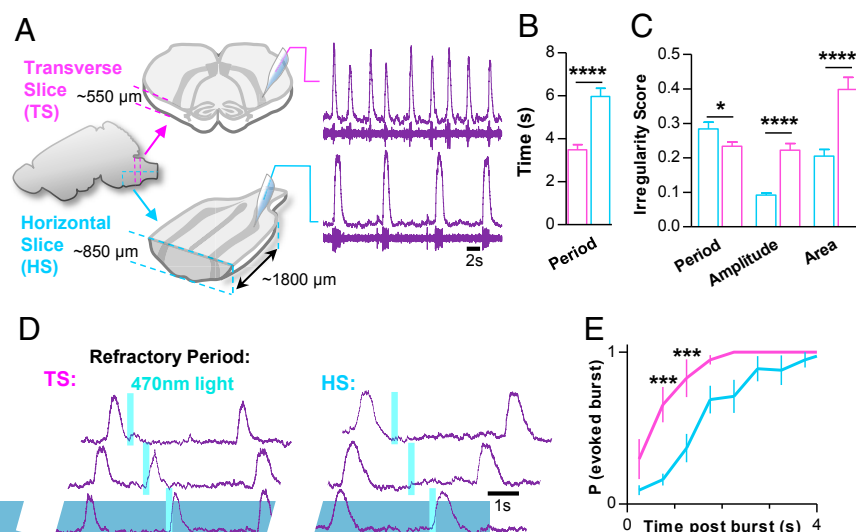


Fig. 1. The intact ventral medullary column produces a more robust inspiratory rhythm than the isolated preBötC. (A) Comparison of population spiking activity recorded from the preBötC in transverse (magenta) and horizontal (cyan) slice preparations. Example raw population spiking (below) and integrated (above) activity is shown for each slice preparation. (B) Group data from $n = 40$ transverse and $n = 41$ horizontal slices comparing inspiratory period and (C) burst-to-burst irregularity scores. (D) Representative optogenetic stimulations in transverse and horizontal slice preparations from Dbx1^{CreERT2};Rosa26^{Chr2} mice showing differences in the refractory period. (E) Quantified probability of photoevoking an inspiratory burst relative to elapsed time following a spontaneous burst in $n = 4$ transverse and $n = 5$ horizontal slices ($*P > 0.05$, $***P > 0.001$, $****P > 0.0001$; means \pm SEM).

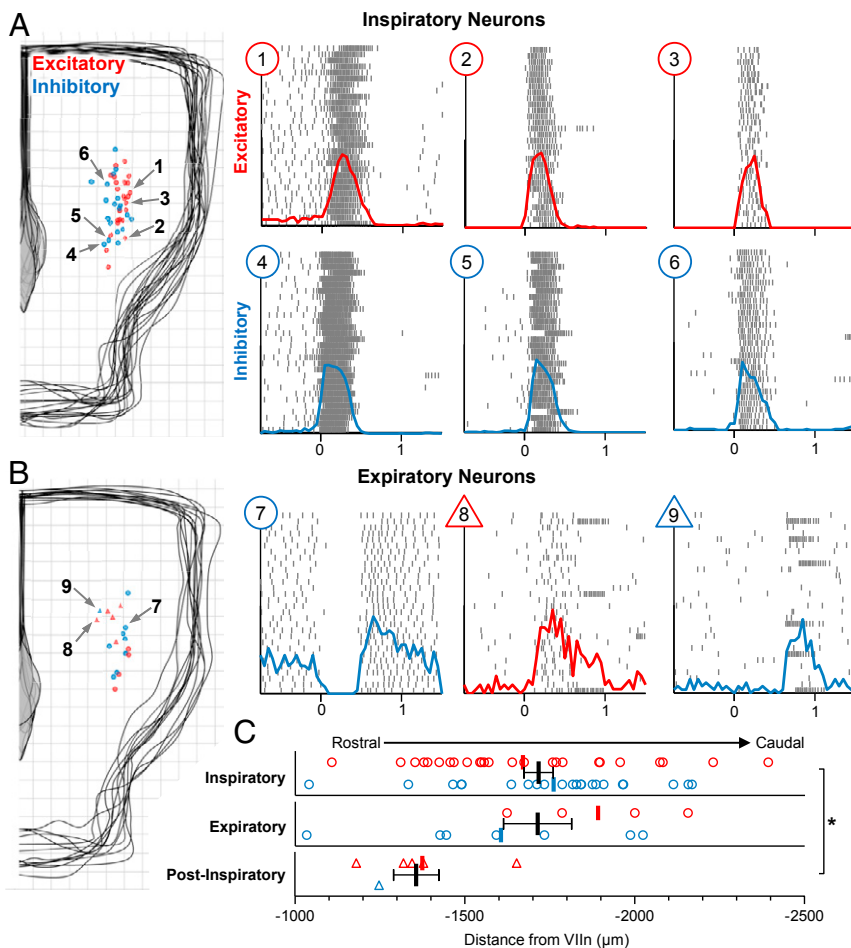


Fig. 2. Spatial and functional characterization of respiratory neurons in the horizontal slice. (A) Locations of 47 inspiratory neurons recorded from 12 horizontal slices (200- μ m grid), and three example excitatory (red; 1–3) and inhibitory (blue; 4–6) neurons. Raster plots show spiking activity over 30 consecutive inspiratory bursts; solid lines show integrated spiking activity (population burst onset at $t = 0$). Note the decrementing spiking pattern of inhibitory neurons. (B) Locations of 12 expiratory and 6 postinspiratory neurons recorded from 6 horizontal slices. Raster plots (Right) show a representative expiratory neuron with modest postinhibitory rebound activity (7), an excitatory postinspiratory neuron that is also active during inspiration (8), and an inhibitory postinspiratory PiCo neuron. Note that strong postinspiratory bursts only occur during some cycles in the absence of norepinephrine. (C) Quantified rostrocaudal locations of excitatory (red) and inhibitory (blue) inspiratory, expiratory, and postinspiratory neurons relative to the VII nerve ($*P < 0.05$; means \pm SEM).

decrementing spiking pattern (neurons 4–6 in Fig. 2A), whereas the spiking pattern of excitatory inspiratory neurons was more variable. Some inspiratory neurons exhibited augmenting spiking activity or a “preinspiratory ramp” before preBötC population bursts, followed by high frequency spiking activity during bursts and were primarily excitatory (five of six neurons). Inspiratory neurons that did not have an obvious preinspiratory ramp were generally silent between preBötC population bursts and varied from augmenting to decrementing and from weakly spiking to strongly spiking during bursts. Despite these general patterns, all inspiratory neurons exhibited considerable cycle-to-cycle stochasticity in spiking onset and activity (46, 56). Under control conditions, functionally active inspiratory neurons were most commonly found near the preBötC center; however, consistent with our extracellular mapping results (SI Appendix, Fig. S1G), inspiratory neurons were found spanning 1.35 mm in the rostrocaudal direction through the ventral medulla.

Neurons active out of phase with the preBötC population, were classified as either expiratory or postinspiratory (Fig. 2B). Similar to previous reports in the isolated preBötC (46), and as predicted by computational models (57), a minority of respiratory neurons along the horizontal slice were expiratory (12 of 65). These neurons exhibited moderate tonic activity between preBötC bursts and were silenced during bursts, and some had modest rebound activity following bursts. Our recordings failed to confirm a rostrocaudal segregation of expiratory and inspiratory neurons (Fig. 2C), as hypothesized by some respiratory models (38, 58). However, postinspiratory neurons were clustered significantly rostral to the preBötC in a region corresponding to the postinspiratory complex (PiCo) (2, 59). Neuromodulation, specifically a low concentration of norepinephrine (NE), is known to facilitate PiCo neurons such that

they fire following every preBötC burst (2). However, the experiments described here were performed in the absence of NE; therefore, PiCo neurons exhibited strong bursts of spiking activity immediately following some, but not all, preBötC bursts (2). PiCo neurons were mostly excitatory (2), although not exclusively (four of five), suggesting that, like the preBötC, the PiCo may be heterogeneous.

Collectively, these data support a network structure that departs from compartmental models of respiratory rhythm generation (58, 60). Inhibitory and excitatory respiratory neurons were not spatially separated into rostral and caudal compartments as often viewed as differentiating the preBötC from the BötC (39, 61). We also did not observe a spatial segregation between inspiratory and expiratory neurons, although postinspiratory neurons were located rostral to the preBötC. Thus, although the density of functionally active inspiratory neurons is likely highest near the preBötC center, we suggest that a distributed network of intermingled excitatory and inhibitory neurons with heterogeneous spiking patterns underlies the inspiratory rhythm.

Inhibition Regulates the Extent of a Dynamic Inspiratory Column. To explore how the balance of excitatory and inhibitory mechanisms may influence the distribution of inspiratory activity, we performed paired recordings in horizontal slices during pharmacological suppression of fast synaptic inhibition. Integrated population activity was recorded at the preBötC and $534 \pm 40 \mu\text{m}$ rostral ($n = 12$) (Fig. 3A). Under baseline conditions, weak irregular inspiratory activity was observed in rostral recordings. However, following suppression of both glycinergic and GABAergic inhibition, integrated population activity in the rostral column increased by $129 \pm 24\%$,

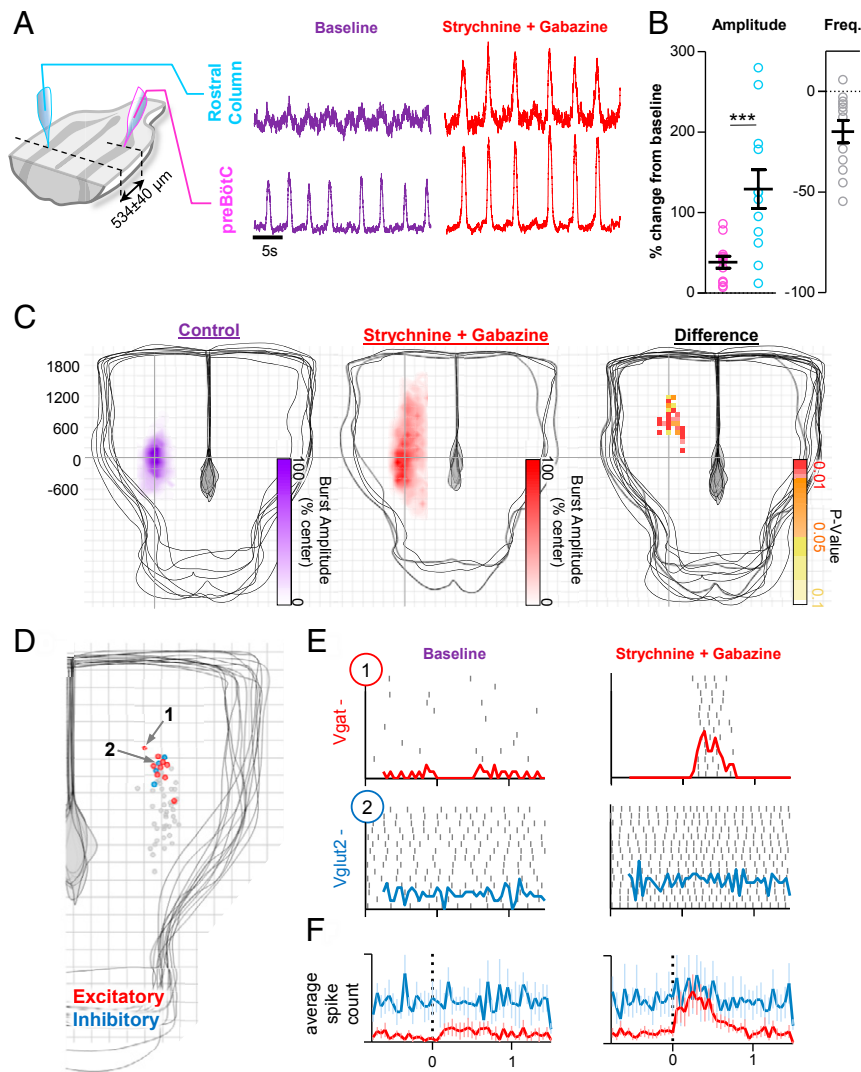


Fig. 3. Inhibitory mechanisms regulate spatial reconfiguration of the inspiratory network. (A) Representative integrated population recordings from the preBötC center and 534 ± 40 μm rostral before (purple) and following suppression of GABAergic and glycinergic inhibition (red). (B) Group data showing changes in burst amplitude and frequency ($n = 12$). (C) Heatmaps (200-μm grid) of inspiratory burst amplitude, across the horizontal slice under control conditions ($n = 8$) and following suppression of synaptic inhibition with strychnine and gabazine ($n = 4$). Differences rostral to the preBötC are shown as a map of Bonferroni-corrected P values. (D) Locations of silent or tonic spiking excitatory (red; $n = 9$) or inhibitory (blue; $n = 4$) neurons recorded rostral of the preBötC. The gray dots indicate the location of neurons with phasic inspiratory activity shown in Fig. 2A. (E) Spike raster plots, for example, excitatory and inhibitory neurons during 15 consecutive inspiratory bursts at baseline and following coapplication of strychnine and gabazine; the solid lines show integrated spiking activity. (F) Average spiking activity of excitatory ($n = 9$) and inhibitory ($n = 4$) neurons at baseline and following suppression of synaptic inhibition ($***P > 0.001$; means ± SEM).

whereas preBötC burst amplitude only increased by $38 \pm 7\%$ (Fig. 3B). The rise slope of inspiratory bursts at the preBötC center increased ($75 \pm 15\%$), and changes in preBötC slope were proportional to changes in rostral burst amplitude (SI Appendix, Fig. S3A). Blockade of inhibition reduced the irregularity of inspiratory bursts in the rostral column, but not at the preBötC center (SI Appendix, Fig. S3B). When glycinergic and GABAergic inhibition were blocked separately, effects on inspiratory burst amplitude were relatively modest (SI Appendix, Fig. S3C). Moreover, effects on inspiratory burst amplitude were dependent on the dose of strychnine and gabazine when applied in combination (SI Appendix, Fig. S3D), suggesting that changes in the rostral extent of inspiratory activity are dependent on the total amount of synaptic inhibition. Increased inspiratory activity along the column following suppression of synaptic inhibition was also associated with a decrease in burst frequency ($-20 \pm 6\%$), likely due to greater synchronization within the network (57) and an increase in the refractory period (43).

Next, inspiratory population activity was systematically mapped in horizontal slices following suppression of synaptic inhibition (Fig. 3C). Heatmaps of burst amplitude were constructed to visualize changes in the distribution of inspiratory activity in the presence and absence of synaptic inhibition. Differences in the distribution of inspiratory activity are displayed as a heatmap of Bonferroni-corrected P values (Fig. 3C). In slices with synaptic

inhibition blocked ($n = 4$), inspiratory activity spanned $2,625 \pm 232 \mu\text{m}$ and was detectable up to $1,575 \pm 93 \mu\text{m}$ rostral of the preBötC, compared with $1,488 \pm 199$ and $625 \pm 106 \mu\text{m}$, respectively, for control slices. Significant differences in integrated inspiratory burst amplitude were localized to the rostral column. Thus, these results indicate that synaptic inhibition within the respiratory network regulates the extent of inspiratory activity rostral to the preBötC.

To shed light on the cellular determinants underlying expansion of inspiratory activity, we tested the influence of synaptic inhibition on nonrespiratory neurons rostral of the preBötC (Fig. 3D–F). Using blind patch-clamp recording, tonic or silent neurons ($n = 13$) located ~ 500 – $600 \mu\text{m}$ rostral of the preBötC center were selected for intracellular recording. Locations of recorded nonrespiratory neurons are plotted in Fig. 3D and quantified in SI Appendix, Fig. S4B. Following blockade of synaptic inhibition with strychnine and gabazine, excitatory neurons (seven of nine) began to discharge bursts of spikes during inspiration (Fig. 3E and F and SI Appendix, Fig. S4A). In contrast, only one of four inhibitory neurons were weakly recruited to spike during inspiration (Fig. 3E and F), suggesting excitatory neurons are preferentially recruited rostral of the preBötC to expand the inspiratory column and that latent excitatory projections from the preBötC to more rostral neurons are revealed following suppression of synaptic inhibition.

Rhythmic Properties of the Inspiratory Column. Excitatory neurons derived from Dbx1-expressing precursors are a critical rhythmic element within the preBötC (33, 44, 45). However, Dbx1 neurons are distributed bilaterally throughout the rostrocaudal extent of the medulla (*SI Appendix, Fig. S1F*). Therefore, we explored the rhythmic properties of Dbx1 neurons along the rostrocaudal axis of the horizontal slice. In Dbx1^{CreERT2}; Rosa26^{ChR2-EYFP} horizontal slices, a 100- μ m-diameter optical fiber was used to stimulate Dbx1 neurons with light (200 ms, 470 nm, 0.5 mW/mm²) at six different locations between 1,500 μ m rostral and 1,000 μ m caudal of the preBötC center, while recording inspiratory activity from the contralateral preBötC. At each location, 50 light stimulations were performed at random time points during the inspiratory cycle (Fig. 4A), and the average probability of evoking a burst at each location was quantified (Fig. 4B). The highest probability of light-evoking contralateral inspiratory bursts was near the preBötC center (92 \pm 10%) and gradually declined as the fiber optic was moved farther rostral or caudal. However, even 1,500 μ m rostral of the preBötC center, there was a 62 \pm 9% chance of evoking a burst. Differences in the probability of evoking bursts were dependent on the time of the stimulus relative to the preceding spontaneous burst (Fig. 4C), suggesting the refractory period of the inspiratory network is more difficult to overcome when activating Dbx1 neurons farther away from the preBötC center, perhaps because the network is more sparse (57). These data also suggest that the threshold for rhythmogenesis is lowest near the preBötC center.

Next, we began to explore the rhythmic properties of different regions of the inspiratory column in isolation. Beginning 100–200 μ m caudal to the VII nerves, four consecutive 550- μ m-thick transverse slices were made from each animal ($n = 9$), two rostral

to the conventional preBötC slice and one caudal (Fig. 4D). Extracellular activity was recorded simultaneously from the caudal surface of all slices. The farthest rostral slices (R1) did not generate spontaneous bursts, whereas spontaneous bursting was generated in four of nine R2 slices, nine of nine preBötC slices, and eight of nine caudal (C) slices. Spontaneous bursting in R2 and C slices was generally very slow and irregular with considerable variability between preparations. The shape of bursts generated by R2 slices resembled bursts generated by preBötC slices, whereas spontaneous bursts generated by C slices were weak with a pronounced decrementing pattern. To mimic excitatory input from the preBötC, we optogenetically stimulated Dbx1 neurons in rostral and caudal slices with light pulses triggered by preBötC bursts, that is, yoked stimulations (Fig. 4E). When Dbx1 neurons were stimulated ipsilateral to the extracellular electrode, bursts were sometimes evoked in R1 slices (43 \pm 17% chance) and always evoked in R2 and C slices. When stimulations occurred contralateral to the extracellular electrode, bursts could not be evoked in R1 slices, were always evoked in R2 slices, and were sometimes evoked C slices (23 \pm 14% chance) (Fig. 4F). In control preparations that did not express ChR2, optogenetic stimulations had no effect (43). The influence of inhibition on each transverse slice was also tested (Fig. 4G and H). Blocking inhibition did not induce bursting in R1 slices. However, in R2 slices that did not burst spontaneously, blocking synaptic inhibition revealed bursting in all slices (four of four); and in R2 slices that did burst spontaneously (206 \pm 110%) but did not in preBötC (–38 \pm 6%; $n = 9$) and C slices (–13 \pm 17%; $n = 9$). Together, these results support the hypothesis that Dbx1 neurons along the rostrocaudal axis of the ventral medulla can contribute to rhythmogenesis and

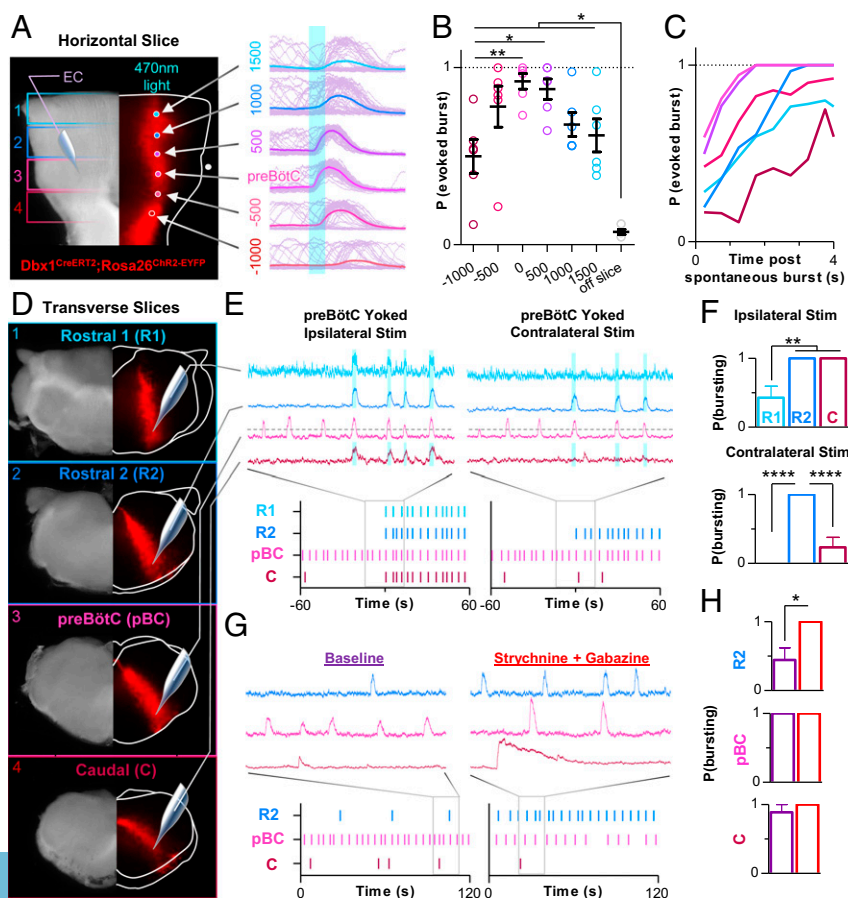


Fig. 4. Rhythmic properties along the inspiratory column. (A) Bright-field (Left) and EYFP fluorescence (Right) images of a Dbx1^{CreERT2};Rosa26^{ChR2-EYFP} horizontal slice showing optogenetic stimulation sites extending from 1,500 μ m rostral to 1,000 μ m caudal of the preBötC and representative integrated population activity (light purple) of the contralateral preBötC during 50 consecutive 200-ms light stimulations (the solid colored lines are averaged traces). (B) Quantified probability of evoking a contralateral preBötC burst at each stimulus location, which was (C) dependent on the elapsed time following a spontaneous preBötC burst (0.5-s bins) ($n = 6$ slices). (D) Representative bright-field and fluorescent images of consecutive transverse slices from a Dbx1^{CreERT2};Rosa26^{ChR2-EYFP} mouse; two rostral (R1 and R2) to the preBötC (pBC) and one caudal (C). (E) Representative integrated population activity and raster plots of bursting during ipsilateral (Left) and contralateral (Right) optogenetic stimulations yoked to preBötC bursting activity, and (F) quantified probability of evoking bursts in each region ($n = 7$ of each slice). (G) Representative population activity and raster plots of spontaneous bursting in R2, pBC, and C slices and following suppression of synaptic inhibition with strychnine and gabazine (1 μ M each). (H) Quantified probability of bursting under spontaneous conditions (purple) and following suppression of inhibition (red) in R2, pBC, and C slices ($n = 9$ of each slice). R1 slices did not burst spontaneously (EC, extracellular) (* $P > 0.05$, *** $P > 0.001$, **** $P > 0.0001$; means \pm SEM).

that synaptic inhibition restrains the rhythmogenic properties of the rostral column.

Sensory Feedback Regulates the Extent of an Inspiratory Column in Vivo. The vagal nerves (X) contain sensory afferents that relay lung stretch information to the respiratory network in the medulla. These afferents create a negative-feedback loop that suppresses inspiratory activity via inhibitory mechanisms within the preBötC (43, 62), thereby preventing overinflation of the lungs (i.e., the Breuer–Hering reflex). Eliminating this vagal-mediated feedback loop reveals a slow, large amplitude breathing pattern (62, 63) and increased refractoriness indicative of a shift in the balance between excitation and inhibition within the preBötC network (43).

To begin to explore how the distribution of inspiratory activity may change in response to alterations in network state, we performed paired extracellular recordings to map multiunit spiking activity along the ventral medulla in spontaneously breathing urethane-anesthetized adult mice (P38–P416; 162 ± 37) (Fig. 5A). One electrode was inserted into the preBötC based on previously established landmarks (43). As expected, robust rhythmic population activity was recorded from this region. Another electrode was positioned rostral to the preBötC center ($558 \pm 20 \mu\text{m}$). At this location, near the rostral “edge” of inspiratory activity, integrated population bursts were smaller and the amplitude was more irregular than at the preBötC center (Fig. 5B and *SI Appendix*, Fig. S5A). After establishing baseline breathing activity in rostral, preBötC, and XII nerve recordings, mice were vagotomized bilaterally ($n = 6$) (Fig. 5B). Similar to previous findings, a large increase in inspiratory motor output from the XII nerve was observed ($278 \pm 93\%$) along with a corresponding decrease in frequency ($-55 \pm 9\%$). Surprisingly, inspiratory activity at the preBötC center was only modestly increased ($13 \pm 6\%$), whereas the amplitude of inspiratory bursts in the rostral region was increased by ($138 \pm 29\%$), over 10 times that observed near the preBötC center (Fig. 5C). Although changes in preBötC burst amplitude were modest, burst rise slope was increased by $35 \pm 8\%$, suggesting network reconfiguration (64). Changes in the slope of the preBötC burst rise had a strong positive linear relationship with changes in rostral burst amplitude (*SI Appendix*, Fig. S5B). Removal of vagal sensory feedback also reduced the irregularity in the amplitude of rostral

bursts ($-32 \pm 8\%$); however, burst amplitude remained more irregular in the rostral column relative to the preBötC center (*SI Appendix*, Fig. S5C).

These results suggested a shift in the distribution of inspiratory activity within the ventral medulla. To further characterize this change in distribution, inspiratory population activity was mapped in control (intact vagus) and vagotomized mice. Beginning at the preBötC center, maximal integrated inspiratory activity was mapped along the ventral medulla and differences between control and vagotomized mice were quantified (Fig. 5D). Cardiorespiratory activity was continuously monitored to ensure potential tissue damage from electrode penetrations had minimal physiological consequences. In control mice ($n = 5$), a small amount of inspiratory activity could be recorded up to $960 \pm 60 \mu\text{m}$ rostral of the preBötC center, whereas in vagotomized mice ($n = 7$) inspiratory activity was detectable up to $1,500 \pm 131 \mu\text{m}$ rostral. Significant differences in integrated inspiratory burst amplitude were isolated to the rostral end of the column. Thus, similar to our observations following suppression of inhibition *in vitro*, there was an anisotropic expansion of inspiratory activity rostral from the preBötC following removal of vagal-mediated sensory feedback *in vivo*.

Gasping and Sighing Along the Inspiratory Column. We next sought to determine how inspiratory activity along the ventral medulla is regulated during different inspiratory behaviors with distinct physiological roles. Under control conditions, the preBötC periodically generates biphasic, large-amplitude, inspiratory bursts that correspond to sighs, and during severe hypoxia, the network is reconfigured to generate bursts that correspond to gasps (65). Utilizing paired extracellular recordings as described above, integrated inspiratory activity was recorded at the preBötC center and $550 \pm 19 \mu\text{m}$ rostral during a transient bout of anoxia in vagus-intact anesthetized mice ($n = 7$) (Fig. 6A). As expected, eupneic activity transformed into gasping with large-amplitude XII bursts ($579 \pm 137\%$) and frequency depression ($-62 \pm 7\%$). In the rostral column, inspiratory burst amplitude was increased by $179 \pm 37\%$ during gasping, whereas at the preBötC center, gasping elicited relatively modest changes in inspiratory burst amplitude ($40 \pm 7\%$) (Fig. 6B) and was associated with a change in burst shape from augmenting to decrementing (*SI Appendix*, Fig. S5D), as indicated by an increase in burst rise slope ($117 \pm 24\%$). The increases in

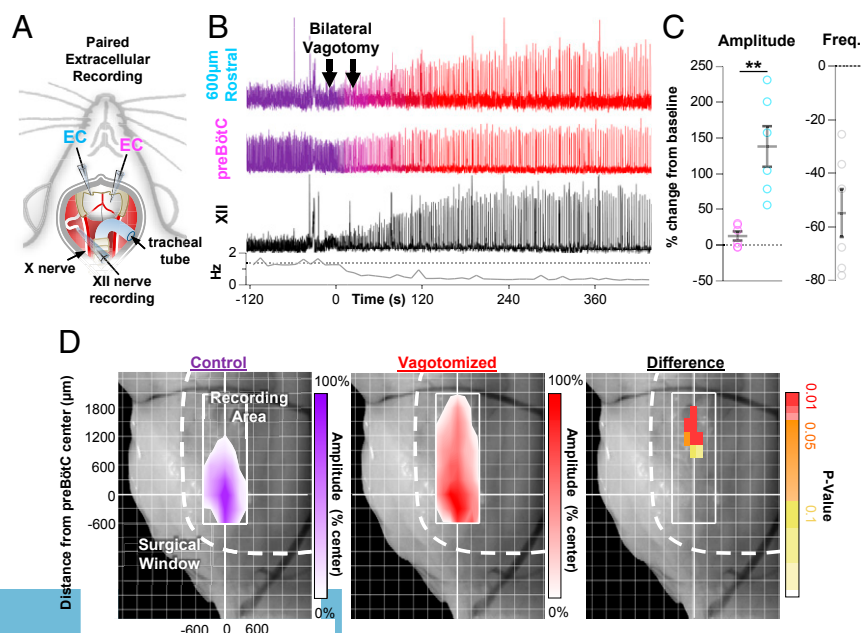


Fig. 5. Vagal sensory feedback restricts inspiratory activity rostral of the preBötC. (A) Schematic of the anesthetized *in vivo* preparation used to perform paired recordings from the ventral medulla and motor output from the XII nerve. (B) Representative experiment showing integrated population recordings of inspiratory activity from 600 μm rostral to the preBötC center (cyan), near the preBötC center (magenta), and from the hypoglossal (XII) nerve (black) under baseline conditions (purple) and following bilateral vagotomy (red). Breathing frequency is shown below (10-s bins). (C) Group data showing changes in burst amplitude and frequency ($n = 6$). (D) Heatmaps of inspiratory activity, as a percentage of preBötC burst amplitude, across the ventral medulla under control conditions ($n = 5$) and following vagotomy ($n = 7$), and the difference shown as Bonferroni-corrected P values ($*P > 0.05$, $**P < 0.01$, $****P > 0.0001$; means \pm SEM).

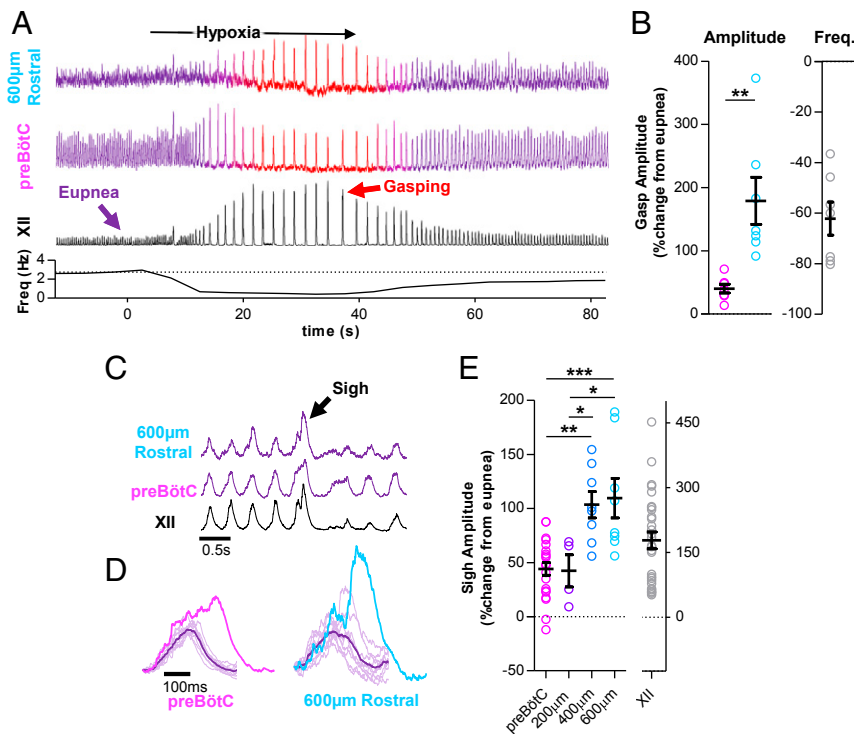


Fig. 6. The spatial distribution of inspiratory activity expands during gasping and sighing in vivo. (A) Representative experiment showing integrated population recordings of inspiratory activity from 600 μm rostral of the preBötC, near the preBötC center, and from the hypoglossal (XII) nerve during a brief bout of anoxia to evoke gasping. Breathing frequency is shown below (10-s bins). (B) Group data showing changes in burst amplitude and frequency ($n = 7$). (C) Representative eupnea and sigh recorded from the preBötC center, 600 μm rostral, and the hypoglossal (XII) nerve, and (D) overlaid eupneic bursts relative to the sigh at each location. (E) Group data of sigh burst amplitude, as a percentage of eupnea amplitude, recorded at the preBötC center and 200, 400, and 600 μm rostral ($*P > 0.05$, $**P > 0.01$, $***P > 0.001$; means \pm SEM).

rostral amplitude were related to changes in preBötC burst rise slope (SI Appendix, Fig. SSE). These experiments indicate that inspiratory activity expands rostrally from the preBötC during gasping in vivo. However, a similar pattern was not observed during “fictive” gasping activity elicited in horizontal slices ($n = 10$). Similar to other in vitro preparations (48), the effects of severe hypoxia on respiratory output were suppressed relative to the in vivo condition. During a transient 5-min episode of anoxia, burst amplitudes during fictive gasping were reduced at both the preBötC center ($-26 \pm 6\%$) and 540 \pm 64 μm rostral of the preBötC ($-15 \pm 8\%$; $P > 0.05$). Frequency depression during fictive gasping ($-24 \pm 7\%$) was also modest compared with gasping in vivo, likely related to, for example, a lack of chemosensory drive from carotid bodies and/or excitatory neuromodulatory inputs that contribute to the hypoxic response in vivo (66–68).

Large-amplitude biphasic inspiratory bursts called sighs occurred spontaneously under control conditions in vagus-intact anesthetized mice (69–71) (Fig. 6 C and D). Sigh burst amplitude was quantified relative to normal inspiratory bursts or “eupnea” (percent change from eupnea) at different rostrocaudal locations along the inspiratory column ($n = 29$ sighs from $n = 6$ animals). Sigh bursts were smaller near the preBötC center ($44 \pm 6\%$) and increased in relative amplitude farther rostral along the inspiratory column ($110 \pm 18\%$ at 600 μm) (Fig. 6E). In the horizontal slice, spontaneous sighs ($n = 9$) were only observed in $n = 5$ slices while performing paired extracellular recordings under control conditions. However, in support of our results in vivo, sigh bursts 363 \pm 62 μm rostral of the preBötC were significantly larger ($68 \pm 11\%$) than at the preBötC center ($39 \pm 3\%$; $P < 0.05$). Thus, the inspiratory column expands rostrally during sighs, suggesting the extent inspiratory activity rostral to the preBötC can change dynamically from cycle to cycle.

Discussion

It is generally thought that breathing is generated by a strictly compartmentalized network within the medulla, with the preBötC being the best-characterized compartment. However, Dbx1-derived inspiratory neurons, the necessary neuronal substrate

underlying rhythm generation in the preBötC, are found along a column that extends rostrally through the BötC and beyond (43, 44). Here, we propose a distributed network structure in which the inspiratory rhythm arises from a dynamically regulated rhythmogenic column containing both the preBötC and the rostrally located BötC, thought to be involved in expiratory rhythmogenesis (38, 39, 60). In our model, the preBötC is defined as the subregion with the lowest threshold for rhythmogenesis; however, the degree to which the preBötC is the exclusive site for rhythmogenesis depends on the metabolic or behavioral context. Our conclusions combine results obtained from reduced slice and intact anesthetized preparations. This approach allowed us to test our hypothesis at the cellular, network, and whole-animal level. However, it is important to emphasize that each experimental approach comes with significant caveats that have been discussed in our previous publications (e.g., refs. 64 and 65). Among these caveats, we would like to point out that slice preparations were performed in neonatal animals at 30 $^{\circ}\text{C}$ and elevated $[\text{K}^+]$ conditions, while the in vivo preparations were performed in adult anesthetized animals. Although each of these preparations provided important insights into the overall conceptual framework, it will be important for future experiments to address how the intact inspiratory network may spatially reconfigure under behavioral conditions such as changes in sleep and wake states.

Our distributed network model is consistent with data from vagotomized cats, in which multielectrode recordings have revealed inspiratory and expiratory neurons with a rich complexity of firing patterns intermingled along the VRC (72–74). This distributed activity has also been observed in sagittal slice preparations from neonatal rodents (48). Here, we identified neurons rostral of the preBötC that are phenotypically and functionally similar to those contained within the conventional “boundaries” of the preBötC (32, 75). Neither inspiratory/expiratory neurons nor excitatory/inhibitory neurons were rostrocaudally segregated between the BötC and preBötC (Fig. 2C), and optogenetic stimulation of excitatory Dbx1 neurons as far as 500–1,500 μm rostral to the preBötC was sufficient to evoke inspiratory bursts (Fig. 4 A and B). In slices that

did not contain the preBötC, bursts could also be evoked by optogenetic stimulations of Dbx1 neurons (Fig. 4 E and F) or by blocking synaptic inhibition (Fig. 4 G and H), suggesting neurons distributed outside of the preBötC can contribute to inspiratory rhythm generation.

Our data indicate that the spatial extent of inspiratory activity is dynamic. This is reminiscent of cortical networks (29, 30), where behaviors are not controlled by one kernel, but rather by distributed sensorimotor networks (76, 77). Furthermore, extensive horizontal connections allow neural activity to spread across the network (29, 30). The spread of activity is controlled by inhibition, and relatively small reductions in the strength of inhibition can result in large changes in the spatial distribution of activity (29). For the respiratory network, we show that inhibition plays a critical role in regulating the spatial extent of inspiratory activity within the network. Suppressing synaptic inhibition led to a large anisotropic expansion of inspiratory activity (Fig. 3). This spatial reconfiguration of activity was controlled by the strength of both GABAergic and glycinergic mechanisms, which may reflect coexpression of these transmitters in many preBötC neurons (78). Removal of sensory feedback inhibition mediated by vagal pulmonary stretch receptors revealed a similar expansion of inspiratory activity rostral to the preBötC (Fig. 5), in accordance with previous demonstrations that this vagal-mediated reflex is ultimately dependent upon inhibitory mechanisms in the ventral medulla (43, 62). We also found that burst-to-burst amplitudes were more irregular farther rostral along the inspiratory column than near the preBötC center, both in vitro and in vivo (SI Appendix, Figs. S3B and S5C), and suppressing inhibition reduced this irregularity. Because in silico models of the preBötC have demonstrated that the regularity of the rhythm depends on the balance between network inhibition and network connectivity (57), we predict that the influence of synaptic inhibition is greater and/or the network is more sparsely connected near the edges of the inspiratory column (Fig. 7). Indeed, blocking synaptic inhibition revealed rhythmic bursting in rostral transverse slices (Fig. 4 G and H), and recruited rostral excitatory neurons to fire during inspiratory bursts (Fig. 3F). Based on these results, we postulate that the number and spatial extent of neurons that contribute to the inspiratory rhythm changes from cycle to cycle depending on a dynamic balance between excitation and inhibition.

The inspiratory network is often described in terms of rhythm- and pattern-generating elements (31, 41) that may change inspiratory burst frequency and amplitude independently or codependently (56). We found that all perturbations that caused the inspiratory column to expand rostrally also resulted in slower rhythms and larger burst amplitudes. Thus, we suggest that spatial reconfiguration of the inspiratory network has codependent effects on inspiratory rhythm and pattern, likely due to recruitment of both rhythm- and pattern-generating elements in the rostral column. Recruitment of more rhythm-generating elements makes the rhythm more robust and synchronized but activates refractory mechanisms, thereby slowing the rhythm, whereas recruitment of more pattern-generating elements contributes to the larger amplitude. However, we emphasize that there may be many neurons with both rhythm- and pattern-generating properties, and the degree to which a given neuron contributes to rhythm vs. pattern generation may change depending on network state (56).

The ability of neuronal networks to spatially reconfigure may be an important property that promotes behavioral flexibility (14, 76, 79). Aside from important neuromodulatory control (16), the flexibility of the breathing rhythm is also regulated by the balance of excitatory and inhibitory mechanisms (53, 56). In the preBötC, hyperactivity of excitatory neurons following blockade of inhibition or vagotomy produces a highly synchronized, slow rhythm with long refractory times and a limited dynamic range (43). Conversely, inhibitory mechanisms reduce the extent of the network and permit rapid breathing frequencies by limiting synchronization and refractory properties of excitatory neurons (43, 53, 57). Thus, we hypothesize that during eupneic breathing, inspiratory activity rostral to the preBötC is suppressed by inhibition to reduce the number of participating neurons and the amount of synchronization during each inspiratory burst (Fig. 7). This mechanism limits the influence of refractory properties and ensures a large dynamic frequency range and increased flexibility, which may be important during changing physiological conditions such as exercise.

By contrast, under severe hypoxia or asphyxia, for example, during airway occlusion, a highly synchronized network may become advantageous as a last resort to promote airway clearance and reoxygenation. During hypoxia-induced gasping, inhibition is suppressed, which reconfigures the network such that it produces a decrementing burst pattern (SI Appendix, Fig. S5D) (14). Here, we show that activity in the rostral column was greatly

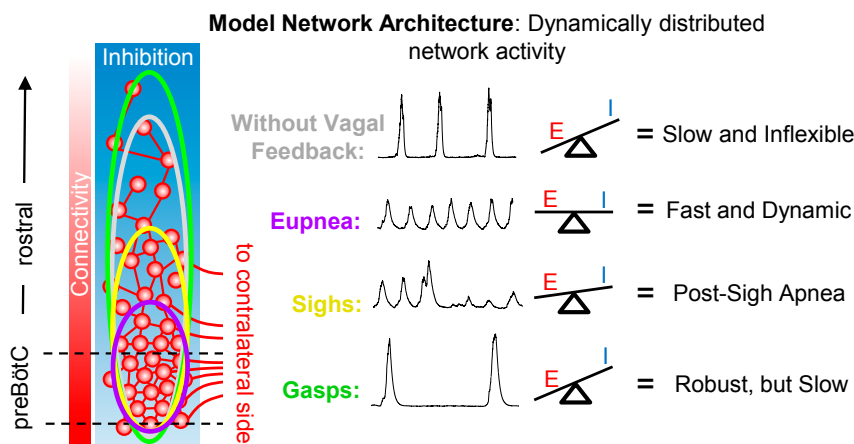


Fig. 7. Hypothesized model for dynamic spatial reconfiguration of inspiratory activity based on a distributed network of excitatory and inhibitory neurons. Gradients of functional connectivity and inhibition determine the threshold for rhythmogenesis, which is lowest in the preBötC. During eupneic breathing (purple), a balance of excitation and inhibition restricts inspiratory activity and permits fast, dynamic rhythmic activity. Suppression of inhibition or removal of vagal sensory feedback (gray) leaves recurrent excitatory mechanisms unrestrained, leading to a rostral expansion of inspiratory activity, hypersynchronization of the network, and a slow inflexible rhythm. During sighs (yellow), a transient increase in excitation during the sigh burst expands the network rostrally resulting in a postsigh apnea. During severe hypoxia or asphyxia, the network is reconfigured to produce gasping (green). Excitatory drive to the network increased and inhibition is suppressed, leading to a large rostral expansion of inspiratory activity and a very robust, but slow, rhythm.

increased during gasping in vivo (Fig. 6A and B). These important network properties may counteract hypoxia-induced suppression of neuronal activity and/or facilitate intrinsic bursting (80–82) to increase synchronization and expand the size of the active network to produce a very robust rhythm in response to severe hypoxia. However, recruiting more neurons into the network and increasing synchronization has consequences, since this will activate refractory mechanisms and slow the rhythm (43). Recruitment of the rostral column during gasping may also provide an explanation for how, in some cases, gasping can be generated after the preBötC is lesioned and eupnea is abolished (50), a finding that is difficult to reconcile with the hypothesis that the preBötC compartment is the exclusive site for gasping (83). In contrast to our in vivo finding, we found a relatively blunted gasping response in vitro (48), which suggests that descending input from the pons, excitatory drive from the carotid body, or neuromodulatory inputs (66, 84) play an important role in generating gasping in vivo.

As mammals evolved, breathing became integrated with an increasing repertoire of behaviors from vocalization to suckling, sniffing, whisking, and chewing (40, 85, 86). As a result, the rhythm-generating network underlying such a widely integrated and vital behavior must be robust, yet also flexible to dynamically adapt breathing to a myriad of state-, metabolic-, and behavioral-dependent demands (87, 88). While the identification of functionally dedicated microcircuits and necessity and sufficiency criterion have guided much of our efforts to understand the neuronal origins of breathing, this approach may miss important characteristics of the network that endow breathing with its remarkable robustness and flexibility.

- Swanson LW, Lichtman JW (2016) From Cajal to connectome and beyond. *Annu Rev Neurosci* 39:197–216.
- Anderson TM, et al. (2016) A novel excitatory network for the control of breathing. *Nature* 536:76–80.
- Eaton RC, DiDomenico R (1985) Command and the neural causation of behavior: A theoretical analysis of the necessity and sufficiency paradigm. *Brain Behav Evol* 27:132–164.
- Tan W, et al. (2008) Silencing preBötzing complex somatostatin-expressing neurons induces persistent apnea in awake rat. *Nat Neurosci* 11:538–540.
- Young RM (1970) *Mind, Brain and Adaptation in the Nineteenth Century: Cerebral Localization and Its Biological Context from Gall to Ferrier* (Oxford Univ Press, New York).
- Seeman SC, et al. (2018) Sparse recurrent excitatory connectivity in the microcircuit of the adult mouse and human cortex. *eLife* 7:e37349.
- Regev A, et al.; Human Cell Atlas Meeting Participants (2017) The human cell atlas. *eLife* 6:e27041.
- Strange BA, Witter MP, Lein ES, Moser EI (2014) Functional organization of the hippocampal longitudinal axis. *Nat Rev Neurosci* 15:655–669.
- Ampatzis K, Song J, Ausborn J, El Manira A (2014) Separate microcircuit modules of distinct v2a interneurons and motoneurons control the speed of locomotion. *Neuron* 83:934–943.
- Gendrel M, Atlas EG, Hobert O (2016) A cellular and regulatory map of the GABAergic nervous system of *C. elegans*. *eLife* 5:e17686.
- Simpson JH, Looger LL (2018) Functional imaging and optogenetics in *Drosophila*. *Genetics* 208:1291–1309.
- Diao F, Elliott AD, Diao F, Shah S, White BH (2017) Neuromodulatory connectivity defines the structure of a behavioral neural network. *eLife* 6:e29797.
- Aso Y, et al. (2014) The neuronal architecture of the mushroom body provides a logic for associative learning. *eLife* 3:e04577.
- Peña-Ortega F (2017) Neural network reconfigurations: Changes of the respiratory network by hypoxia as an example. *Adv Exp Med Biol* 1015:217–237.
- Weimann JM, Marder E (1994) Switching neurons are integral members of multiple oscillatory networks. *Curr Biol* 4:896–902.
- Doi A, Ramirez JM (2008) Neuromodulation and the orchestration of the respiratory rhythm. *Respir Physiol Neurobiol* 164:96–104.
- Ramirez JM, et al. (2012) The cellular building blocks of breathing. *Compr Physiol* 2:2683–2731.
- Koch H, Garcia AJ, 3rd, Ramirez JM (2011) Network reconfiguration and neuronal plasticity in rhythm-generating networks. *Integr Comp Biol* 51:856–868.
- Getting PA (1989) Emerging principles governing the operation of neural networks. *Annu Rev Neurosci* 12:185–204.
- Kupfermann I, Weiss KR (2001) Motor program selection in simple model systems. *Curr Opin Neurobiol* 11:673–677.
- Arnold AEGF, Ekstrom AD, Iaria G (2018) Dynamic neural network reconfiguration during the generation and reinstatement of mnemonic representations. *Front Hum Neurosci* 12:292.

Our investigations of inspiratory rhythm generation in the intact VRC suggest that the preBötC and BötC form a distributed inspiratory column of excitatory and inhibitory neurons that allows the size of the active network to be dynamically controlled. Working as one, the preBötC and BötC may overcome the trade-off between a region's specialization and its capacity for network reconfiguration (89), thereby permitting robust and flexible breathing. The ability of distributed neuronal networks to spatially reconfigure may be a general property that bestows animals with the ability to adapt behaviors to continuous and often rapid changes in their internal and external environment.

Methods

All experiments and animal procedures were approved by the Seattle Children's Research Institute's Animal Care and Use Committee and conducted in accordance with the National Institutes of Health guidelines. Male and female mice were selected randomly based on litter distributions. Protocols for in vitro (2, 43, 57, 64) and in vivo (32, 43) preparations, as well as optogenetic, electrophysiological, and pharmacological manipulations (2, 43, 64, 65, 70, 82, 90, 91) were performed as described previously. Detailed descriptions of the methods and data analysis are provided in *SI Appendix*, and a summary of the statistical tests used is provided in *SI Appendix*, Table S1.

ACKNOWLEDGMENTS. We are grateful for NIH Grants R01 HL126523 (awarded to J.-M.R.), P01 HL 090554 (awarded to J.-M.R.), K99 HL145004 (awarded to N.A.B.), and F32 HL134207 (awarded to N.A.B.) for funding this project.

- Berkowitz A, Roberts A, Soffe SR (2010) Roles for multifunctional and specialized spinal interneurons during motor pattern generation in tadpoles, zebrafish larvae, and turtles. *Front Behav Neurosci* 4:36.
- Bolser DC, Poliacek I, Jakus J, Fuller DD, Davenport PW (2006) Neurogenesis of cough, other airway defensive behaviors and breathing: A holoarchitectural system? *Respir Physiol Neurobiol* 152:255–265.
- Kristan WB, Jr, Shaw BK (1997) Population coding and behavioral choice. *Curr Opin Neurobiol* 7:826–831.
- Kouchtir-Devanne N, Capaday C, Cassim F, Derambure P, Devanne H (2012) Task-dependent changes of motor cortical network excitability during precision grip compared to isolated finger contraction. *J Neurophysiol* 107:1522–1529.
- Sanes JN, Donoghue JP (2000) Plasticity and primary motor cortex. *Annu Rev Neurosci* 23:393–415.
- Morton DW, Chiel HJ (1994) Neural architectures for adaptive behavior. *Trends Neurosci* 17:413–420.
- Braun U, et al. (2015) Dynamic reconfiguration of frontal brain networks during executive cognition in humans. *Proc Natl Acad Sci USA* 112:11678–11683.
- Capaday C, van Vreeswijk C, Ethier C, Feringhoff-Borg J, Weber D (2011) Neural mechanism of activity spread in the cat motor cortex and its relation to the intrinsic connectivity. *J Physiol* 589:2515–2528.
- Capaday C, et al. (2009) On the nature of the intrinsic connectivity of the cat motor cortex: Evidence for a recurrent neural network topology. *J Neurophysiol* 102:2131–2141.
- Feldman JL, Kam K (2015) Facing the challenge of mammalian neural microcircuits: Taking a few breaths may help. *J Physiol* 593:3–23.
- Ruangkittisakul A, Kottick A, Picardo MC, Ballanyi K, Del Negro CA (2014) Identification of the pre-Bötzing complex inspiratory center in calibrated "sandwich" slices from newborn mice with fluorescent Dbx1 interneurons. *Physiol Rep* 2:e12111.
- Wang X, et al. (2014) Laser ablation of Dbx1 neurons in the pre-Bötzing complex stops inspiratory rhythm and impairs output in neonatal mice. *eLife* 3:e03427.
- Koshiya N, Smith JC (1999) Neuronal pacemaker for breathing visualized in vitro. *Nature* 400:360–363.
- Smith JC, Ellenberger HH, Ballanyi K, Richter DW, Feldman JL (1991) Pre-Bötzing complex: A brainstem region that may generate respiratory rhythm in mammals. *Science* 254:726–729.
- Ezure K, Tanaka I, Kondo M (2003) Glycine is used as a transmitter by decrementing expiratory neurons of the ventrolateral medulla in the rat. *J Neurosci* 23:8941–8948.
- Feldman JL, Loewy AD, Speck DF (1985) Projections from the ventral respiratory group to phrenic and intercostal motoneurons in cat: An autoradiographic study. *J Neurosci* 5:1993–2000.
- Smith JC, Abdala AP, Borgmann A, Rybak IA, Paton JF (2013) Brainstem respiratory networks: Building blocks and microcircuits. *Trends Neurosci* 36:152–162.
- Smith JC, Abdala AP, Rybak IA, Paton JF (2009) Structural and functional architecture of respiratory networks in the mammalian brainstem. *Philos Trans R Soc Lond B Biol Sci* 364:2577–2587.
- Ramirez JM, Dashkevskiy T, Marlin IA, Baertsch N (2016) Microcircuits in respiratory rhythm generation: Commonalities with other rhythm generating networks and evolutionary perspectives. *Curr Opin Neurobiol* 41:53–61.

41. Del Negro CA, Funk GD, Feldman JL (2018) Breathing matters. *Nat Rev Neurosci* 19: 351–367.
42. Del Negro CA, Hayes JA (2008) A “group pacemaker” mechanism for respiratory rhythm generation. *J Physiol* 586:2245–2246.
43. Baertsch NA, Baertsch HC, Ramirez JM (2018) The interdependence of excitation and inhibition for the control of dynamic breathing rhythms. *Nat Commun* 9:843.
44. Bouvier J, et al. (2010) Hindbrain interneurons and axon guidance signaling critical for breathing. *Nat Neurosci* 13:1066–1074.
45. Gray PA, et al. (2010) Developmental origin of preBötzinger complex respiratory neurons. *J Neurosci* 30:14883–14895.
46. Carroll MS, Viemari JC, Ramirez JM (2013) Patterns of inspiratory phase-dependent activity in the in vitro respiratory network. *J Neurophysiol* 109:285–295.
47. Lindsey BG, Segers LS, Shannon R (1987) Functional associations among simultaneously monitored lateral medullary respiratory neurons in the cat. II. Evidence for inhibitory actions of expiratory neurons. *J Neurophysiol* 57:1101–1117.
48. Barnes BJ, Tuong CM, Mellen NM (2007) Functional imaging reveals respiratory network activity during hypoxic and opioid challenge in the neonate rat tilted sagittal slab preparation. *J Neurophysiol* 97:2283–2292.
49. Zuperku EJ, et al. (June 28, 2018) Inputs to medullary respiratory neurons from a pontine subregion that controls breathing frequency. *Respir Physiol Neurobiol*, 10.1016/j.resp.2018.06.011.
50. Ramirez JM, Schwarzacher SW, Pierrefiche O, Olivera BM, Richter DW (1998b) Selective lesioning of the cat pre-Bötzinger complex in vivo eliminates breathing but not gasping. *J Physiol* 507:895–907.
51. Neumueller S, et al. (2011) Anatomic changes in multiple brainstem nuclei after incremental, near-complete neurotoxic destruction of the pre-Bötzinger complex in adult goats. *Respir Physiol Neurobiol* 175:1–11.
52. Krause KL, et al. (2009) Normal breathing pattern and arterial blood gases in awake and sleeping goats after near total destruction of the presumed pre-Bötzinger complex and the surrounding region. *J Appl Physiol* 106:605–619.
53. Ramirez JM, Baertsch NA (2018a) The dynamic basis of respiratory rhythm generation: One breath at a time. *Annu Rev Neurosci* 41:475–499.
54. Kottick A, Del Negro CA (2015) Synaptic depression influences inspiratory-expiratory phase transition in Dbx1 interneurons of the preBötzinger complex in neonatal mice. *J Neurosci* 35:11606–11611.
55. Winter SM, et al. (2009) Glycinergic interneurons are functionally integrated into the inspiratory network of mouse medullary slices. *Pflügers Arch* 458:459–469.
56. Ramirez JM, Baertsch N (2018b) Defining the rhythmogenic elements of mammalian breathing. *Physiology (Bethesda)* 33:302–316.
57. Harris KD, et al. (2017) Different roles for inhibition in the rhythm-generating respiratory network. *J Neurophysiol* 118:2070–2088.
58. Molkov YI, Rubin JE, Rybak IA, Smith JC (2017) Computational models of the neural control of breathing. *Wiley Interdiscip Rev Syst Biol Med* 9:e1371.
59. Anderson TM, Ramirez JM (2017) Respiratory rhythm generation: Triple oscillator hypothesis. *F1000 Res* 6:139.
60. Rybak IA, Abdala AP, Markin SN, Paton JF, Smith JC (2007) Spatial organization and state-dependent mechanisms for respiratory rhythm and pattern generation. *Prog Brain Res* 165:201–220.
61. Smith JC, Abdala AP, Koizumi H, Rybak IA, Paton JF (2007) Spatial and functional architecture of the mammalian brain stem respiratory network: A hierarchy of three oscillatory mechanisms. *J Neurophysiol* 98:3370–3387.
62. Janczewski WA, Tashima A, Hsu P, Cui Y, Feldman JL (2013) Role of inhibition in respiratory pattern generation. *J Neurosci* 33:5454–5465.
63. Clark FJ, von Euler C (1972) On the regulation of depth and rate of breathing. *J Physiol* 222:267–295.
64. Lieske SP, Thoby-Brisson M, Telgkamp P, Ramirez JM (2000) Reconfiguration of the neural network controlling multiple breathing patterns: Eupnea, sighs and gasps [see comment]. *Nat Neurosci* 3:600–607.
65. Peña F, Parkis MA, Tryba AK, Ramirez JM (2004) Differential contribution of pacemaker properties to the generation of respiratory rhythms during normoxia and hypoxia. *Neuron* 43:105–117.
66. Morris KF, et al. (2018) Carotid chemoreceptors tune breathing via multipath routing: Reticular chain and loop operations supported by parallel spike train correlations. *J Neurophysiol* 119:700–722.
67. Rybak IA, et al. (2004) Modelling respiratory rhythmogenesis: Focus on phase switching mechanisms. *Adv Exp Med Biol* 551:189–194.
68. Guyenet PG (2014) Regulation of breathing and autonomic outflows by chemoreceptors. *Compr Physiol* 4:1511–1562.
69. Ramirez JM (2014) The integrative role of the sigh in psychology, physiology, pathology, and neurobiology. *Prog Brain Res* 209:91–129.
70. Tryba AK, et al. (2008) Differential modulation of neural network and pacemaker activity underlying eupnea and sigh-breathing activities. *J Neurophysiol* 99: 2114–2125.
71. Li P, et al. (2016) The peptidergic control circuit for sighing. *Nature* 530:293–297.
72. Lindsey BG, et al. (1994) Distributed actions and dynamic associations in respiratory-related neuronal assemblies of the ventrolateral medulla and brain stem midline: Evidence from spike train analysis. *J Neurophysiol* 72:1830–1851.
73. Abbott SB, Stornetta RL, Coates MB, Guyenet PG (2011) Phox2b-expressing neurons of the parafacial region regulate breathing rate, inspiration, and expiration in conscious rats. *J Neurosci* 31:16410–16422.
74. Segers LS, et al. (2012) Discharge identity of medullary inspiratory neurons is altered during repetitive fictive cough. *Front Physiol* 3:223.
75. Ruangkittisakul A, et al. (2008) Generation of eupnea and sighs by a spatiochemically organized inspiratory network. *J Neurosci* 28:2447–2458.
76. Brovelli A, et al. (2017) Dynamic reconfiguration of visuomotor-related functional connectivity networks. *J Neurosci* 37:839–853.
77. Auffret M, et al. (2018) Optogenetic stimulation of cortex to map evoked whisker movements in awake head-restrained mice. *Neuroscience* 368:199–213.
78. Oke Y, Miwakeich F, Oku Y, Hirrlinger J, Hülsmann S (2018) Cell type-dependent activation sequence during rhythmic bursting in the preBötzinger complex in respiratory rhythmic slices from mice. *Front Physiol* 9:1219.
79. Hearne LJ, Cocchi L, Zalesky A, Mattingley JB (2017) Reconfiguration of brain network architectures between resting-state and complexity-dependent cognitive reasoning. *J Neurosci* 37:8399–8411.
80. Peña F (2009) Neuronal network properties underlying the generation of gasping. *Clin Exp Pharmacol Physiol* 36:1218–1228.
81. Richter DW, Bischoff A, Anders K, Bellingham M, Windhorst U (1991) Response of the medullary respiratory network of the cat to hypoxia. *J Physiol* 443:231–256.
82. Peña F, Ramirez JM (2004) Substance P-mediated modulation of pacemaker properties in the mammalian respiratory network. *J Neurosci* 24:7549–7556.
83. St John WM (2009) Noeud vital for breathing in the brainstem: Gasping—yes, eupnoea—doubtful. *Philos Trans R Soc Lond B Biol Sci* 364:2625–2633.
84. Izumizaki M, Pokorski M, Homma I (2004) Role of the carotid bodies in chemosensory ventilatory responses in the anesthetized mouse. *J Appl Physiol* (1985) 97:1401–1407.
85. Moore JD, et al. (2013) Hierarchy of orofacial rhythms revealed through whisking and breathing. *Nature* 497:205–210.
86. Milsom WK (2010) Adaptive trends in respiratory control: A comparative perspective. *Am J Physiol Regul Integr Comp Physiol* 299:R1–R10.
87. Mateika JH, Duffin J (1994) Coincidental changes in ventilation and electromyographic activity during consecutive incremental exercise tests. *Eur J Appl Physiol Occup Physiol* 68:54–61.
88. Ramirez JM, et al. (2013) Central and peripheral factors contributing to obstructive sleep apneas. *Respir Physiol Neurobiol* 189:344–353.
89. Chai LR, Mattar MG, Blank IA, Fedorenko E, Bassett DS (2016) Functional network dynamics of the language system. *Cereb Cortex* 26:4148–4159.
90. Vong L, et al. (2011) Leptin action on GABAergic neurons prevents obesity and reduces inhibitory tone to POMC neurons. *Neuron* 71:142–154.
91. Kottick A, Martin CA, Del Negro CA (2017) Fate mapping neurons and glia derived from Dbx1-expressing progenitors in mouse preBötzinger complex. *Physiol Rep* 5: e13300.